Physica B 657 (2023) 414811

Contents lists available at ScienceDirect

Physica B: Condensed Matter

journal homepage: www.elsevier.com/locate/physb

Promising high temperature thermoelectric performance of layered oxypnictide YZnAsO

Subhajit Sau, Sushree Sarita Sahoo, Arul Raj Natarajan, V. Kanchana *

Department of Physics, Indian Institute of Technology Hyderabad, Kandi 502285, Sangareddy, Telangana, India

ARTICLE INFO

Keywords:
1111 compounds
Phonon dispersion
Lattice thermal conductivity
Thermoelectric properties
Figure of merit

ABSTRACT

Thermoelectric materials can convert heat into electricity directly via the Seebeck effect, providing an alternative to global energy demands. Here we present mechanical, dynamical, and thermoelectric properties of YZnAsO, a quaternary oxypnictide, in the framework of Density Functional Theory. The low value of Debye temperature (θ_D=308.29K) and high value of the Grüneisen parameter (~1.77) hint for low lattice thermal conductivity (k_l), and this is supported by the computed value of ~0.4 W/mK at 800 K. The electronic transport coefficients are computed using Boltzmann transport equation beyond the constant relaxation time approximation (CRTA) including different scattering mechanisms. While the power factor for hole doping is higher along 'a', the k_l is extremely low along 'c', resulting in a high figure of merit (ZT) along 'c'. Hence, we predict YZnAsO as a promising n-type oxide thermoelectric owing to its low k_l with a high ZT = 1.07 at 800 K with 15% maximum thermoelectric efficiency.

1. Introduction

Because of escalating energy consumption and global environmental degradation due to pollution, hunt for clean, environmentally sustainable and renewable energy resources have become primary focus and a networthy scientific study issue. Dwindling supply of fossil fuels are redirecting us to search for new energy sources. Renewable energy is preferable, but it is insufficient, and alternative energy sources must be developed. Only then major concerns like worldwide energy crisis, rising of surface temperature, effects of climate change can be mitigated. During the energy conversion process, a significant amount of energy (~72%) is squandered as heat in industries, automobiles, and other sources of waste [1]. As a result, there is an urgent need to transform waste heat into usable energy in order to enhance energy efficiency and minimize consumption. Thermoelectric materials are a type of functional material that, through the seebeck effect, may effectively create energy from waste heat. Therefore, they can be incorporated into power generation and cooling devices. Thermoelectric (TE) technologies are unique and can offer potential solutions to the prevailing issues as they are capable of direct or reversible energy conversion between thermal and electrical power from unrecoverable sources. TE efficiency can be measured by a dimensionless figure of merit $ZT = S^2\sigma T/\kappa$, where S is Thermopower (also known as Seebeck coefficient), σ is the electrical conductivity, T is the absolute temperature, and κ is the total thermal conductivity, a sum of the electronic(κ_e) and lattice thermal conductivity (κ_l). S, σ, κ_e cannot be tuned seperately as they have complex interdependence with carrier concentration and depends on electronic structure, whereas κ_l depends on the structure and bonding of the material. Three strategies can further enhance ZT: increasing the power factor (PF = $S^2\sigma$) i.e promoting electron transport, decreasing κ i.e impeding thermal transport, or tuning both concurrently. As both S and σ exhibits opposite behavior with respect to carrier concentration n, 10^{19}–10^{20} cm^{-3} concentration range gives maximized PF by balancing S and σ for most of the semiconductors [2]. S and σ tied up by the relation $S \propto \sigma^{0.25}$. Apart from n, ZT of bulk TE materials possibly can be enhanced to a much higher level by electronic structure and microstructure tailoring (e.g., band flattening, increasing number of band extrema, modulation doping [2]). Layered materials draw attention due to their intrinsic ultralow lattice thermal conductivities and large Seebeck coefficients [3,4]. BiCuSeO [5] and LaCuSeO [3] are the best example for layered potential thermoelectric materials. The discovery of low-temperature superconductivity in $LaFeAsO_{1-x}F_x$ ($0.05 < x < 0.12$) has drawn attention on ZrCuSiS type of oxyarsenides. They were found to host good thermoelectric properties at low temperatures with doping, which finds application as a cooling material in liquid-nitrogen temperature range [6–8]. Later, many more iron-based oxyarsenides were also explored for elemental substitutional effects on their superconducting nature and thermoelectric properties [9–15]. The notable change in 'S' is attributed to a change in electronic structure. ZrCuSiAs family also draws attention as varieties of phenomenon

* Corresponding author.
E-mail address: kanchana@phy.iith.ac.in (V. Kanchana).

https://doi.org/10.1016/j.physb.2023.414811
Received 18 August 2022; Received in revised form 14 February 2023; Accepted 10 March 2023
Available online 11 March 2023

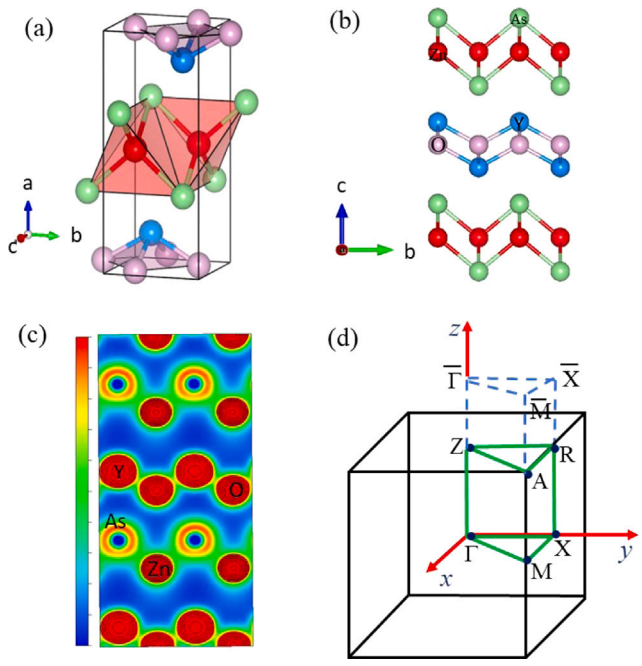

Fig. 1. Optimized structure (a); Y, Zn, As and O atoms are shown in blue, red, green and pink, layered form of the structure (b), charge density along (100) plane (c); in the color bar blue color denotes decrease in charge and red color increase in charge, and Brillouin Zone (d) for YZnAsO.

like diamagnetism [16], ferromagnetism [17,18], semiconducting and metallic antiferromagnetism [19,20], Mott transition [21], magnetoresistance [21] arises due to chemical flexibility. Recently, Chang et al. reported 49% increase in ZT value by reduction of oxygen. They found $BiCuTeO_{0.88}$ displayed a $ZT_{max} = 1.06$ at 673 K, surpassing the ZT value of pristine $BiCuTeO_{1.00}$ by 49% (ZT_{max} = 0.71 at 723 K) [22]. Till now, several superior and high performance thermoelectric materials have been reported [23,24]; however, practical application are limited by factors like high cost or toxicity [25]. In this regard, advantages like abundance, cost-effective, environmentally friendly manufacturing, oxidization resistance, high thermal and chemical stability makes oxide based materials as promising alternative candidate. As a result, the search of new oxide based high performance TE materials needs to be investigated for 'greener' options [26–29].

Here we present layered YZnAsO as promising thermoelectric materials. Some previous studies report YZnAsO as the potential material for optical properties [30]. Our work aims to give a proper insight into the different mechanical, dynamical and thermoelectric properties of YZnAsO. The electron relaxation time has been estimated using two approximations named momentum relaxation time approximation(MRTA) and self-energy relaxation time approximation(SERTA) to calculate the absolute thermoelectric coefficients. Different scattering mechanisms such as acoustic deformation scattering (ADP), ionized impurity scattering (IMP) and polar optical scattering (POP) are included in calculating the scattering rates for various temperatures. The paper is formatted as follows: the methodology is given in Section 2, followed by Section 3, which discuss about the stability of the investigated compound along with thermal conductivity. Sections 4 & 5 explain the electronic structure and thermoelectric properties, and the summary is given in Section 6.

2. Computational details

The structural geometry optimization is done with GGA-PBE [31] exchange correlation functional using the Vienna Ab-initio Simulation Package(VASP) code [32–34]. As this is a layered compound we included van der Waals effect with DFT-D3 method [35]. We have considered the pseudopotentials with valence electron configuration: $4d^1 5s^2$ for Y, $3d^{10}4s^2$ for Zn, $3d^{10}4s^2 4p^3$ for As, $2s^2 2p^4$ for O. The energy and force tolerance factors are chosen to be 10^{-6} eV and 0.01 eV/Å, respectively along with plane-wave energy cutoff of 600 eV. A Monkhorst–Pack grid of 18 × 18 × 8 is used to relax the structures [36]. Phonon band spectrum is calculated using the combination of PHONOPY code [37] and force constants estimated by density functional perturbation theory(DFPT) [38] in VASP. The effective phonon frequency was estimated as a weighted sum of all Γ-point phonon modes to capture the scattering from entire phonon band structure. Lattice thermal conductivity calculations was performed using phono3py package [39] by calculating the 2nd and 3rd order inter-atomic force constants (IFCs). Thermoelectric properties and scattering rates are calculated using AMSET [40].

Table 1
Calculated and experimental values of lattice parameters of YZnAsO.

Compound	YZnAsO		
	Theo.	Exp. [42]	Exp. [43]
a (in Å)	3.93	3.94	3.94
c (in Å)	8.88	8.84	8.84
c/a	2.25	2.24	2.24
V (in $Å^3$)	137.86	137.48	137.38
Zn-As (in Å)	2.55	–	–
Y-O (in Å)	2.25	–	–
As-Zn-As (deg)	100.85	–	–

3. Structural, mechanical and dynamical properties

The crystal structure of the tetragonal phase of YZnAsO belongs to the space group P4/nmm (129), with Z = 2 per unitcell (ZrCuSiAs type) which is shown in Fig. 1(a). Table 1 summarizes the optimized equilibrium lattice constants computed with reported experimental data for YZnAsO. From the table it can be inferred that our computation matches well with the experimentally available values. For each atom coordination number is 4. For this structure $[YO]^{1+}$ layers are sandwiched between $[ZnAs]^{1-}$ layers forming ABAB sequence and edge shared $ZnAs_4$ tetrahedra along the tetragonal(c) axis. Both the layers have mixed ionic–covalent nature (Fig. 1(c) green and yellow region) due to in-plane charge transfer and inter-layer bonding is completely ionic in nature indicated by blue region and the same nature is also presented by a previous study through bader analysis [41]. The unit cell contains 2 As atoms with coordinates As (3/4, 3/4, z_{As}) and (1/4, 1/4, 1 − z_{As}) where optimized z_{As} value is 0.317. Zn–As bond length (l) is 2.55 Å and As–Zn–As bond angles(α) is 100.85°. Considering this, the relation between these values and lattice parameters of tetragonal 1111-type structures is given by $a = 2l.\sin(\alpha/2)$, $c = (2l/(1 - 2z_{As}))\cos(\alpha/2)$.

The elastic constants and phonon dispersion of YZnAsO were further computed to better understand its mechanical and dynamical properties. For tetragonal single-crystal structure(with Laue class 4/mmm) there are only 6 independent elastic constants which are tabulated in Table 2, and they satisfy Born's stability criteria [44,45]. Elastic constants C_{11} and C_{33} characterize the resistance against the compressional strains along the principal crystalline directions respectively, while C_{44} and C_{66} characterize the resistance to shear deformations. The measure of the elastic anisotropy is given by difference between C_{11} and C_{33}. With single-crystal elastic constants, one may derive macroscopic elastic moduli as well as polycrystalline elastic properties including bulk(B), shear, and Young's modulus (E). Here, Shear modulus (G_H) is the average of shear moduli G_V and G_R derived using Voigt and Ruess approximation, respectively, as per Hill's average [46]. Bulk modulus, which is closely related to the binding energy of atoms in a crystal and can be used as a standard to evaluate average bond

Table 2
Calculated elastic constants (C_{ij}), Young Modulus (GPa), Bulk Modulus (in GPa), Sound Velocities (v_l, v_t, v_m; in km/s), Poisson's ratio (ν), Grüneisen parameter(γ), and Debye Temperature (θ_D in K).

Elastic constants	YZnAsO
C_{11}	175.90
C_{12}	35.73
C_{13}	37.91
C_{33}	107.20
C_{44}	17.86
C_{66}	40.26
E_H	87.28
B_H	74.0
G_H	33.54
B/G	2.20
v_l	4.54
v_t	2.41
v_m	2.69
ν	0.3
γ	1.77
Θ_D	308.29

strength, influences the hardness of the material, i.e., the ability of material volume to resist elastic deformation. Pugh's modulus ratio (B/G) indicates the material's ductility or brittleness and Shear modulus represents resistance to plastic deformation. B/G ratio for YZnAsO is greater than the "critical" value of 1.75, indicating the ductile behavior of the compound. Poisson's ratio(ν) of this compound also confirms the ductile nature of this compound according to Frantsevich's rule, i.e., the value of ν greater than 0.6 indicates the ductile nature [47]. Using Poisson's ratio, we have also computed the Grüneisen parameter (γ) for YZnAsO, and its value is 1.77 [48]. Grüneisen parameter reflects the deviation of phonon vibrations of a crystal from harmonic oscillation so it is considered as an anharmoniticity parameter. Our calculated Grüneisen parameter is comparable to BiCuSeO [49], LaZnAsO [50] and PbTe [51] having values 1.5, 1.14 and 1.45 respectively. The calculated Debye temperature of YZnAsO is 308.29 K whereas BiCuSeO has 243 K [49]. Thus, low Θ_D and high γ give the possibility of low lattice thermal conductivity (κ_l) which is favorable for obtaining high ZT value.

The phonon band spectrum projected along high symmetry path of BZ is presented in Fig. 2(a). There are no negative modes for any wave vector in the crystal structure in its reference state, indicating that it is a dynamically and energetically stable structure. Low-frequency modes are comprised of heavier materials, whereas high-frequency modes are comprised of lighter elements. The discrepancy in atomic weights is responsible for the gap between low and high frequency optical modes. The low-frequency phonon modes play a significant role in κ_l values. Next, we have estimated temperature dependent κ_l, and the same is displayed in Fig. 6(c). κ_l decreases with temperature due to enhancement in phonon scattering with temperature, and this behavior is quite obvious. The values of lattice thermal conductivity are determined by Debye temperature values and phonon band dispersion. It is known that κ_l is connected to phonon group velocity (V_g) and phonon relaxation time (τ) by the following relation,

$$k_l = \frac{1}{3} V_g^2 \tau \tag{1}$$

The frequency dependent phonon-lifetime is given in Fig. 2(b). We observed that the lifetime of most of the phonon modes exists in the low-frequency region below 6 THz. In general, acoustic modes are mainly responsible for lattice thermal conductivity. In our case maximum acoustic phonon frequency is ~4 THz, below this frequency lifetime is low with a sparse and sporadic peak at 4 THz which is due to interaction between low-lying optical phonons and acoustical phonons. For most of the phonons, lifetime is below 10 ps which is relatively low. The interaction of optical and acoustic phonon modes along 'a' direction induces more phonon–phonon scattering and higher V_g. From Fig. 2(c,d) we note that V_g along 'c' is lower compared to 'a' direction leading to low k_l in 'c' direction so we can expect lower k_l along 'c'. The computed lattice thermal conductivity values are low 0.97 W/m K along 'c' at T = 300 K, which is favorable for thermoelectric applications. A comparison of k_l with the other prototype structures is shown in Table 5.

4. Electronic structure properties and scattering lifetime

We have computed its electronic structure properties to get a physical insight of YZnAsO. YZnAsO is a direct bandgap semiconductor as the top of conduction band minima and valence band maxima are lying at the Γ- point [Fig. 3]. However, the band gap measured experimentally is 1.9 eV [43], whereas GGA band gap is 1.2 eV. Due to unphysical self-Coulomb repulsion [52], PBE functional underestimate the electronic band gap. We have introduced the TB-mBJ functional as implemented in the WIEN2k [53] program to improve the band gap, and obtained electronic band gap of 1.8 eV (direct). The total density of states (DOS) and orbital contributions of the individual atoms in the compound are presented in [Fig. 3(b)]. From the plot, it is evident that the valence band is mainly dominated by As - p and Zn - d orbitals, whereas the conduction band is mainly occupied by Y - d and Zn - s orbitals with a modest mixing of other states. The electron pockets can be seen at high symmetry points 'Γ', 'M' and 'A' around 1.2 eV, and these pockets might play a crucial role for thermoelectric properties with heavy electron doping at high temperatures. The similar features were also found in prototype structure BiCuSeO for holes [54].

As YZnAsO is a layered structure, we cleaved the crystal structure along the z-direction and gave a vaccum of 12 Å on each side in order to avoid interlayer interactions. To determine the stability of a monolayer, we compute the material's exfoliation energy, which is defined as the amount of energy necessary to separate an atomic layer from the bulk. The exfoliation energy is determined to be −2.47 eV/atom. We also calculate band and phonon dispersion for monolayered YZnAsO [Fig. 4]. Positive phonon frequencies confirms the stability of the layered structure. As the $[YO]^{1+}$ and $[ZnAs]^{1-}$ are charged layers, a small amount of charge flow between these substructures is obvious and we can expect a metallic nature which is also confirmed by the crossing of only two bands near Fermi level from the band dispersion [Fig. 4(a)]. The rise of band gap in bulk might be due to hybridization between these substructres while building the solid from these building blocks [55].

We used the Boltzmann transport theory within the AMSET code [40] to evaluate the thermopower (S), electronic conductivity (σ), and power factor ($S^2\sigma$) to calculate ZT. AMSET goes beyond the constant relaxation time approximation (CRTA), which provides simplest description of the collision kernel while ignoring interaction mechanisms. CRTA just indicates that collisions occur, but it makes no mention of the scattering mechanisms. We derived scattering rates based on three different electron–phonon coupling scattering processes. Acoustic deformation potential (ADP) and ionized impurity imparted by coulomb potential are elastic, whereas polar optical-phonon (POP) scattering is inelastic. POP is created by atoms vibrating against one other in the unit cell, while ADP is caused by intrinsic deviation from periodicity in a perfect crystal induced by thermal vibrations of atoms traveling in the same direction. These scattering rates are useful for calculating relaxation time, which is further used to calculate different transport coefficients. Elastic scattering processes are treated with Momentum relaxation time approximation(MRTA) and described by Fermi-Golden Rule,

$$\tau^{-1}_{n\mathbf{k}\to m\mathbf{k+q}} = \frac{2\pi}{\hbar}|g_{nm}(\mathbf{k},\mathbf{q})|^2\delta(\Delta\varepsilon^{nm}_{\mathbf{k},\mathbf{q}}) \tag{2}$$

In the Inelastic process, where scattering occurs via emission or absorption of phonon, is described by a similar kind of equation under SERTA,

$$\tau^{-1}_{n\mathbf{k}\to m\mathbf{k+q}} = \frac{2\pi}{\hbar}|g_{nm}(\mathbf{k},\mathbf{q})|^2 \times [(n_{\mathbf{q}} + 1 - f^0_{m\mathbf{k+q}})\delta(\Delta\varepsilon^{nm}_{\mathbf{k},\mathbf{q}} - \hbar\omega_{\mathbf{q}})$$

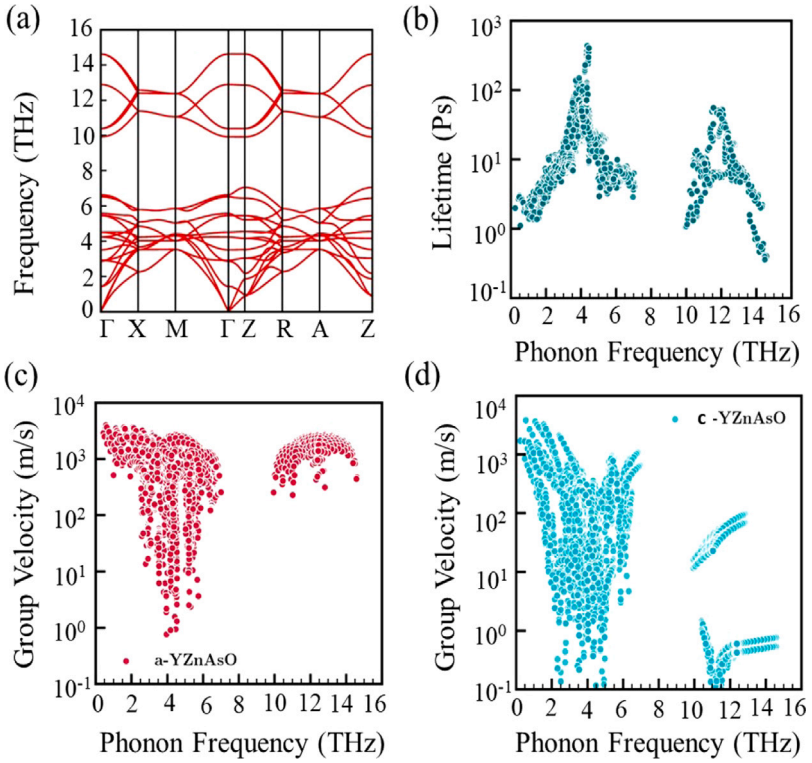

Fig. 2. (a) Phonon dispersion (b) phonon lifetime and (c,d) phonon group velocity along 'a' and 'c' direction of YZnAsO.

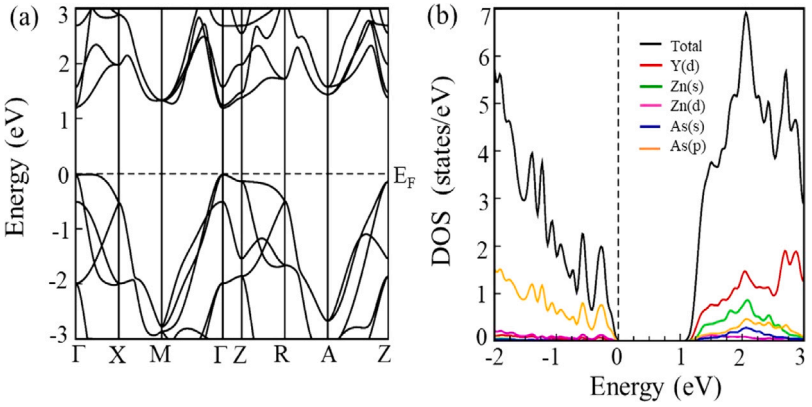

Fig. 3. (a) Band structure and (b) DOS of bulk YZnAsO.

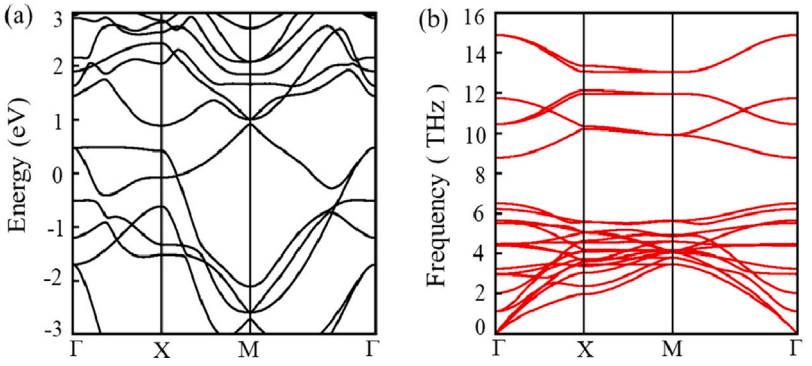

Fig. 4. (a) Band structure and (b) Phonon dispersion of monolayered YZnAsO.

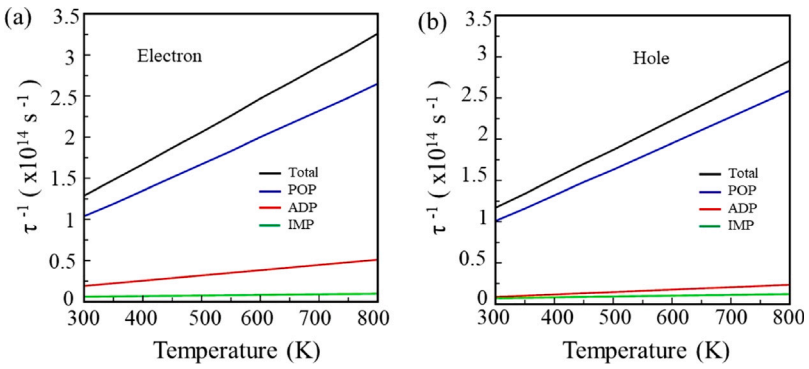

Fig. 5. Temperature dependent scattering rates of YZnAsO.

Table 3
Born effective charges of the elements.

Charges	Y	Zn	As	O
Nominal	+3	+2	−3	−2
Z^*_{xx}	4.69	1.97	−3.52	−3.5
Z^*_{zz}	4.95	0.86	−1.96	−3.85

Table 4
Effective mass of holes and electrons in the unit of mass of electron(m_0).

Path	m^*_h	m^*_e
$\Gamma - X$	−10.20	0.26
$\Gamma - Z$	−6.00	1.37

Table 5
Comparison of lattice thermal conductivity at 300 K and ZT value of YZnAsO with other oxide based TE materials. (k_{la} and k_{lc} are lattice thermal conductivities along 'a' and 'c' directions respectively).

Compounds	k_{la}	k_{lc}	ZT
BiCuSeO (Theo.) [57,58]	1.16	0.52	0.92 (900 K)
BiCuTeO (Expt.) [22]	$k_{l,av} = 0.55$	–	0.71 (723 K)
LaCuSeO (Theo.) [3]	2.51	0.18	2.71 (900 K)
LaZnAsO (Theo.) [50]	7	1.9	1.92 (1000 K)
CsAgO (Theo.) [59]	0.12	0.18	1.44 (800 K)
YZnAsO (Present work)	32.39	0.97	1.07 (800 K)

$$+ (n_{\mathbf{q}} + f^0_{m\mathbf{k}+\mathbf{q}})\delta(\Delta\varepsilon^{nm}_{\mathbf{k},\mathbf{q}} + \hbar\omega_{\mathbf{q}})] \tag{3}$$

where, $-\hbar\omega_{\mathbf{q}}$ and $+\hbar\omega_{\mathbf{q}}$ correspond to scattering by emission and absorption of a phonon, respectively.

The inputs for AMSET are uniform band structure, wave function coefficients, 6 × 6 elastic tensors (C_{ij}), deformation potentials, static (ϵ_s) and high-frequency dielectric (ϵ_∞) constants, and effective phonon frequency (= 5.44 THz) are calculated from VASP. Calculated values of the above mentioned quantities are tabulated below

$$\epsilon_s = \begin{bmatrix} 34.33 & 0 & 0 \\ 0 & 34.33 & 0 \\ 0 & 0 & 20.78 \end{bmatrix}, \epsilon_\infty = \begin{bmatrix} 22.68 & 0 & 0 \\ 0 & 22.68 & 0 \\ 0 & 0 & 12.71 \end{bmatrix}$$

Different scattering mechanisms contributing to the scattering rate at a concentration of 10^{20} cm^{-3} is shown in Fig. 5. The trend shows that POP is dominating scattering mechanism, which can be attributed to high Born effective charges (Table 3) [56].

5. Thermoelectric properties

The low lattice thermal conductivity of YZnAsO intends us to compute the thermoelectric properties. The thermoelectric properties are calculated as a function of temperature at different carrier concentration along 'a' and 'c' directions to observe anistropic nature as the system is tetragonal. The thermopower for both carriers is shown in Fig. 7. Thermopower for holes is higher compared to electrons, as seen from plots. It decreases as we increase the doping concentration implying the absence of bipolar conduction effect in the optimum concentration region. Also S for hole along 'a' is higher compared to 'c' and for electron it is higher along 'c'. The difference between S values may be due to the difference in effective masses of the carrier (Table 4).

For hole doping concentration 1×10^{19} cm^{-3} thermopower reaches to a very high value ~400 μV/K along 'a' direction but the calculated electrical conductivity is very high (~62 000 S/cm) for doping concentration 1×10^{20} cm^{-3} and shows huge anisotropic nature and same trend found for electron doping also. This behavior of σ can be explained by the fact that the inter-layer charge transfer is very low than intra-layer charge transfer as we have discussed in Section 1. The same anisotropic nature is also visible in the power factor, which reaches maximum value along 'a' for both hole and electron doping concentration 1×10^{20} cm^{-3} due to the dominant behavior of electrical conductivity. Further, we obtain a Figure of merit(ZT), a measure of thermoelectric efficiency. Despite having large S and σ for hole doping along 'a', large lattice thermal conductivity along 'a' deteriorates the ZT value. We found that electron doping has comparatively higher power factor than hole doping and low thermal conductivity along 'c', leading to a good ZT value. ZT value is 0.18 at room temperature, which is enhanced up to 1.07 at 800 K [Fig. 8].

Finally using the figure of merit, efficiency of TE device can be calculated using the formula

$$\eta = \frac{T_H - T_C}{T_H} \frac{\sqrt{1+ZT}-1}{\sqrt{1+ZT}+T_C/T_H} \tag{4}$$

where, T_C and T_H are temperature of cold and hot junctions. Considering $T_C = 300$ K and $T_H = 800$ K maximum value of TE device efficiency is 15%.

As seen, ZT is strongly temperature-dependent mainly due to a decrease of lattice thermal conductivity and on thermopower at elevated temperatures. Because S is proportional to temperature and at high temperature increased lattice vibrations, obstruct heat-conducting phonons, lowering lattice thermal conductivity. We observed the electronic part also exhibits weaker temperature dependence [Fig. 6(a,b)]. Since, σ is anisotropic k_e is anisotropic too as $k_e = L\sigma T$, where L is the Lorenz number. Along with the values of k_l, a comparison of the ZT of YZnAsO and the available experimental and theoretical ZT values of a few other compounds are shown in Table 5. The computed ZT value is comparable to that of a few other known oxide materials [22,58,60–63].

6. Conclusion

In summary, we have discussed structural, dynamical, electronic, elastic properties and transport mechanisms for YZnAsO using first-principle calculations. The studied compound is a direct bandgap semiconductor whose stability is confirmed by elastic coefficients and the

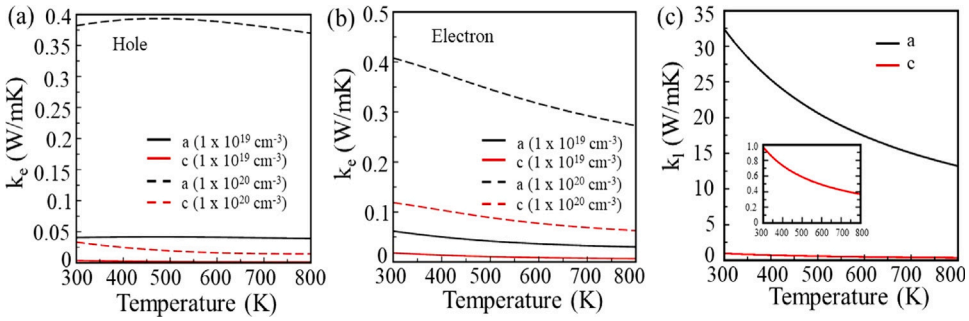

Fig. 6. Electronic and lattice thermal conductivity of YZnAsO.

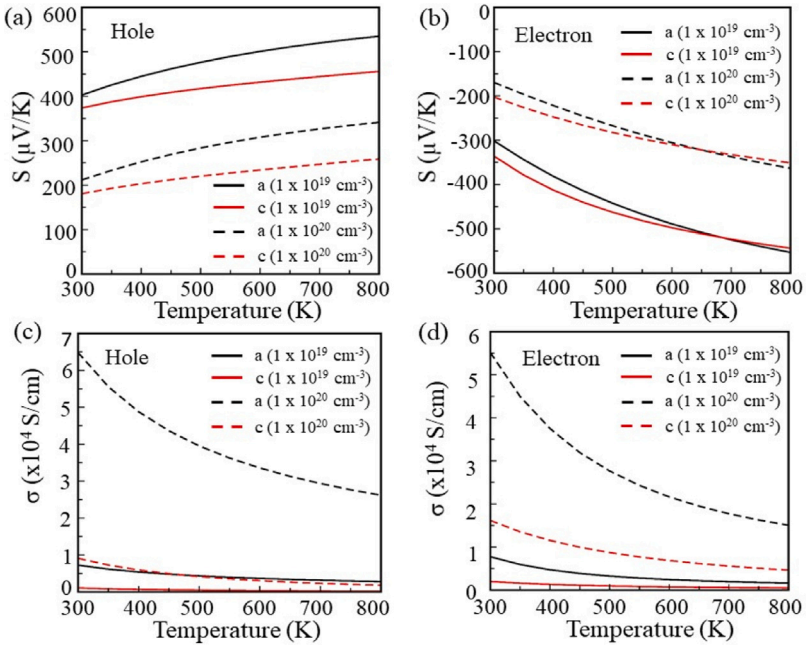

Fig. 7. Seebeck coefficient(S) (a,b), electrical conductivity(σ) (c,d) of YZnAsO.

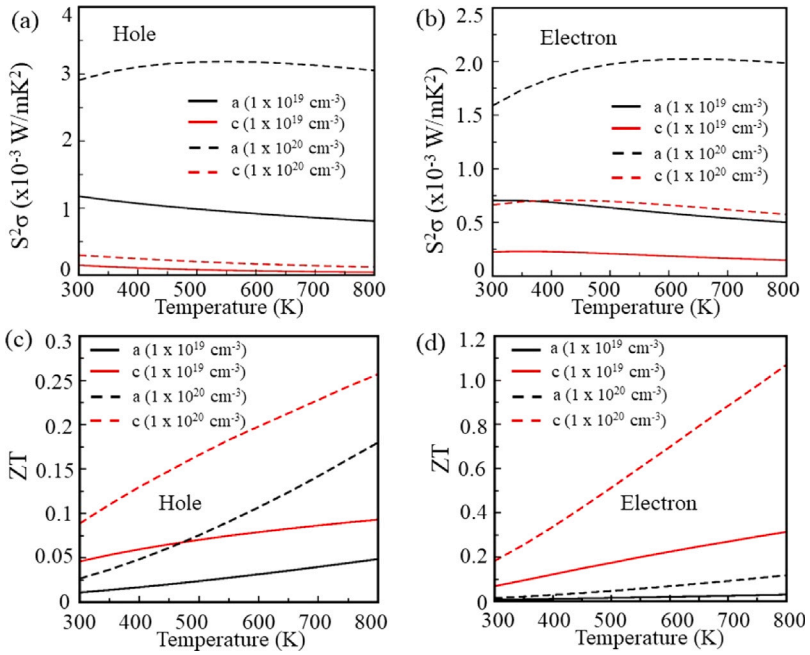

Fig. 8. Power factor (a,b), Figure of merit (c,d) of YZnAsO.

absence of imaginary phonon modes. We further calculated the transport coefficients in the temperature range 300–800 K through analysis of thermopower(S) and electrical conductivity as a function of T. YZnAsO showed good thermoelectric performance at high temperature with a ZT value of 1.07 at 800 K along 'c' direction. Additionally, strain effects, chemical doping might be a possible route to improve the thermoelectric performance as found in BiCuSeO [64]. Overall, the examined system is an excellent n-type thermoelectric material that may be further explored for various device applications.

CRediT authorship contribution statement

Subhajit Sau: Performed all the calculations, Analyzed the data, Manuscript preparation. **Sushree Sarita Sahoo:** Data analysis, Manuscript editing. **Arul Raj Natarajan:** Manuscript editing, Discussion of results. **V. Kanchana:** Formulating the problem, Analysis and discussion of results, Funding, Supervision.

Declaration of competing interest

The authors declare that they have no known competing financial interests or personal relationships that could have appeared to influence the work reported in this paper.

Data availability

Data will be made available on request.

Acknowledgments

The authors Subhajit Sau, Sushree Sarita Sahoo, Arul Raj Natarajan and V. Kanchana would like to thank IIT Hyderabad for providing computational facilities. Subhajit Sau would like to thank MHRD for fellowship. Both Sushree Sarita Sahoo and V Kanchana would like to acknowledge CSIR, India, project with sanction No. (03(1433)/18/EMR-II) for financial support. Arul Raj Natarajan would like to thank CSIR for fellowship. The authors would like to acknowledge National Supercomputing Mission (NSM) for providing computing resources of PARAM SEVA at IIT Hyderabad, which is implemented by C-DAC and supported by the Ministry of Electronics and Information Technology (MeitY), India and the Department of Science and Technology (DST), Government of India. All the authors confirmed the final manuscript.

References

[1] Clemens Forman, Ibrahim Kolawole Muritala, Robert Pardemann, Bernd Meyer, Renew. Sustain. Energy Rev. 57 (2016) 1568–1579.
[2] Gangjian Tan, Li-Dong Zhao, Mercouri G. Kanatzidis, Chem. Rev. 116 (2016) 12123–12149.
[3] Ning Wang, Menglu Li, Haiyan Xiao, Xiaotao Zu, Liang Qiao, Phys. Rev. A 13 (2020) 024038.
[4] Fancy Qian Wang, Yaguang Guo, Qian Wang, Yoshiyuki Kawazoe, Puru Jena, Chem. Mater. 29 (2017) 9300–9307.
[5] Li-Dong Zhao, Jiaqing He, David Berardan, Yuanhua Lin, Jing-Feng Li, Ce-Wen Nanc, Nita Dragoe, Energy Environ. Sci. 7 (2014) 2900–2924.
[6] Yoichi Kamihara, Takumi Watanabe, Masahiro Hirano, Hideo Hosono, J. Am. Chem. Soc. 130 (11) (2008) 3296–3297.
[7] David Bérardan, Loreynne Pinsard-Gaudart, Nita Dragoe, J. Alloys Compd. 481 (2009) 470–472.
[8] Loreynne Pinsard-Gaudart, David Bérardan, Julien Bobroff, Nita Dragoe, Phys. Status Solidi (RRL) 2 (4) (2008) 185–187.
[9] C. Wang, Y.K. Li, Z.W. Zhu, S. Jiang, X. Lin, Y.K. Luo, S. Chi, L.J. Li, Z. Ren, M. He, H. Chen, Y.T. Wang, Q. Tao, G.H. Cao, Z.A Xu, Phys. Rev. B 79 (2009) 054521.
[10] G.F. Chen, Z. Li, D. Wu, G. Li, W.Z. Hu, J. Dong, P. Zheng, J.L. Luo, N.L. Wang, Phys. Rev. Lett. 100 (2008) 247002.
[11] Z.A. Ren, J. Yang, W. Lu, W. Yi, G.C. Che, X.L. Dong, L.L. Sun, Z.X Zhao, Mater. Res. Innov. 12 (2008) 105.
[12] Zhi-An Ren, et al., Europhys. Lett. 82 (2008) 57002.
[13] CHEN Gen-Fu, Li Zheng, W.U. Dan, et al., Chin. Phys. Lett. 25 (2008) 2235–2238.
[14] P. Cheng, L. Fang, H. Yang, X. Zhu, G. Mu, H. Luo, Z. Wang, H.H Wen, Sci. China, Ser. G 51 (2008) 719.
[15] Lin-Jun Li, Yu-Ke Li, Zhi Ren, Yong-Kang Luo, Xiao Lin, Mi He, Qian Tao, Zeng-Wei Zhu, Guang-Han Cao, Zhu-An Xu, Phys. Rev. B 78 (2008) 132506.
[16] Rainer Pottgena, Dirk Johrendt, Z. Nat. 63b (2008) 1135–1148.
[17] Hiroshi Yanagi, Ryuto Kawamura, Toshio Kamiya, Yoichi Kamihara, Masahiro Hirano, Tetsuya Nakamura, Hitoshi Osawa, Hideo Hosono, Phys. Rev. B 77 (2008) 224431.
[18] G. Xu, et al., Europhys. Lett. 82 (2008) 67002.
[19] Sean Muir, M.A. Subramanian, Prog. Solid State Chem. 40 (2012) 41–56.
[20] Michael A. McGuire, Andrew F. May, Brian C. Sales, J. Solid State Chem. 191 (2012) 71–75.
[21] Y. Shiomi, S. Ishiwata, Y. Taguchi, Y Tokura, Phys. Rev. B 84 (2011) 054519.
[22] H.C. Chang, T.H. Chen, R. Sankar, Y.J. Yang, L.C. Chen, K.H Chen, Mater. Today Phys. 15 (2020) 100248.
[23] S. Nag, A. Dhar, A. Gupta, Exhaust heat recovery using thermoelectric generators: A review, in: D. Srivastava, A. Agarwal, A. Datta, R. Maurya (Eds.), Advances in Internal Combustion Engine Research, Springer, Singapore, 2018.
[24] L.D. Zhao, S.H. Lo, Y. Zhang, H. Sun, G. Tan, C. Uher, C. Wolverton, V.P. Dravid, M.G. Kanatzidis, Nature 508 (2014) 373–377.
[25] G. Ren, J. Lan, C. Zeng, Y. Liu, B. Zhan, S. Butt, Y.H. Lin, C.W Nan, JOM 67 (2015) 211–221.
[26] J.U. Rahman, N.V. Du, W.H. Nam, W.H. Shin, K.H. Lee, W.S. Seo, M.H. Kim, S. Lee, Sci. Rep. 9 (2019) 8624.
[27] S.G. Tan, H. Lei, D.F. Shao, H.Y. Lv, W.J. Lu, Y.N. Huang, Y. Liu, B. Yuan, L. Zu, X.C. Kan, W.H. Song, Y.P Sun, Appl. Phys. Lett. 105 (2014) 082109.
[28] J.S. Cha, S.M. Choi, G.H. Kim, S.J. Kim, K Park, Ceram. Int. 44 (2018) 6376–6383.
[29] J.F. Li, W.S. Liu, L.D. Zhao, M. Zhou, NPG Asia Mater. 2 (2010) 152–158.
[30] S.H.I. Yi-ming, Y.E Shao-long, J. Cent. South Univ. Technol. 18 (2011) 998–1003.
[31] J.P. Perdew, K. Burke, M. Ernzerhof, Phys. Rev. Lett. 77 (1996) 3865–3868.
[32] G. Kresse, J. Furthmüller, Phys. Rev. B 54 (1996) 11169–11186.
[33] G. Kresse, J. Furthmuller, Comput. Mater. Sci. 6 (1996) 15–50.
[34] G. Kresse, H. Hafner, Phys. Rev. B 47 (1993) 558–561.
[35] S. Grimme, J. Antony, S. Ehrlich, H Krieg, J. Chem. Phys. 132 (2010) 154104.
[36] H.J. Monkhorst, J.D. Pack, Phys. Rev. B 13 (1976) 5188–5192.
[37] T. Atsushi, T. Isao, Scr. Mater. 108 (2015) 1–5.
[38] G. Xavier, L. Changyol, Phys. Rev. B 55 (1997) 10355.
[39] A. Togo, L. Chaput, I Tanaka, Phys. Rev. B 91 (2015) 094306.
[40] A.M. Ganose, J. Park, A. Faghaninia, et al., Nature Commun. 12 (2021) 2222.
[41] V.V Bannikov, Mater. Chem. Phys. 116 (2009) 129–133.
[42] Andre T. Nientiedt, Wolfgang Jeitschko, Inorg. Chem. 37 (3) (1998) 386–389.
[43] Hannes Lincke, Robert Glaum, Volker Dittrich, Manfred H. Möller, Rainer Pöttgen, Anorg. Allg. Chem. 635 (2009) 936–941.
[44] M. Born, K. Huang, Acta Cryst. 9 (1956) 837–838.
[45] Felix Mouhat, Francois-Xavier Coudert, Phys. Rev. B 90 (2014) 224104.
[46] R Hill, Proc. Phys. Soc. Lond. A 65 (1952) 349.
[47] I.N. Frantsevich, F.F. Voronov, S.A. Bakuta, Handbook on Elastic Constants and Moduli of Elasticity for Metals and Nonmetals, Naukova Dumka, Kiev, 1982.
[48] V.N. Belomestnykh, E.P. Tesleva, Interrelation between anharmonicity and lateral strain in quasi-isotropic polycrystalline solids, Tech. Phys. 49 (2004) 1098–1100.
[49] Yan-Ling Pei, Jiaqing He, Li Jing-Feng, Fu Li, Qijun Liu, Wei Pen, Barreteau Celine, Berardan David, Nita Dragoe, Li-Dong Zhao, NPG Asia Mater. 5 (2013) e47.
[50] Maud Einhorn, Benjamin A.D. Williamson, David O. Scanlon, J. Mater. Chem. A 8 (2020) 7914.
[51] M.C. Roufosse, P.G. Klemens, Thermal conductivity of complex dielectric crystals, Phys. Rev. B 7 (1973) 5379–5386.
[52] J.P. Perdew, Alex Zunger, Phys. Rev. B 23 (1981) 5048–5079.
[53] P. Blaha, K. Scwarz, P. Sorantin, S.B. Tricky, Comput. Phys. Comm. 59 (1990) 399–415.
[54] Celine Barreteau, David Be rardan, Emilie Amzallag, LiDong Zhao, Nita Dragoe, Chem. Mater. 24 (16) (2012) 3168–3178.
[55] S. Lebegue, Phys. Rev. B 75 (2007) 035110.
[56] Jifeng Sun, David J. Singh, APL Mater. 4 (2016) 104803.
[57] Gang Liu, Hongyi Sun, Jian Zhou, Qingfang Li, X.G. Wan, J. Appl. Phys. 119 (2016) 185109.
[58] Daifeng Zou, Shuhong Xie, Yunya Liu, Jianguo Lin, Jiangyu Li, J. Mater. Chem. A 1 (2013) 8888.
[59] Vineet Kumar Sharma, V. Kanchana, Mayanak K. Gupta, Ranjan Mittal, J. Phys.: Condens. Matter 34 (2022) 295502.
[60] S. Walia, S. Balendhran, H. Nili, S. Zhuiykov, G. Rosengarten, Q. Wang, M. Bhaskaran, S. Sriram, M. Strano, K. Kalantar-zadeh, Prog. Mater. Sci. 58 (2013) 1443–1489, English(US).
[61] H.C. Chang, T.H. Chen, R. Sankar, Y.J. Yang, L.C. Chen, K.H. Chen, Mater. Today Phys. 15 (2020) 100248.
[62] K. Fujita, T. Mochida, K Nakamura, Japan. J. Appl. Phys. 40 (2001) 4644–4647.
[63] S.A. Miller, P. Gorai, U. Aydemir, T.O. Mason, V. Stevanoviæ, E.S. Toberer, G.J. Snyder, J. Mater. Chem. C 5 (2017) 8854–8861.
[64] Rui Tan, Chunpeng Zou, Kai Pan, Daifeng Zou, Yunya Liu, J. Alloys Compd. 743 (2018) 610–617.